



Wearable, fabric-based microfluidic systems with integrated electrochemical and colorimetric sensing array for multiplex sweat analysis

Sekar Madhu, Md. Sajjad Alam, Sriramprabha Ramasamy, Jungil Choi*

Department of Mechanical Engineering, Ajou University, Suwon 16499, Republic of Korea

ARTICLE INFO

Keywords:

Carbon fabric
Microfluidics
pH sensor
Sweat sensor
Wearable device

ABSTRACT

Wearable sweat sensors enable continuous, real-time, non-invasive detection of sweat analytes, providing valuable insights for personalized health monitoring. Despite recent advances, non-invasive sweat monitoring has yet to reach its full analytical potential. The amalgamation of electrochemical and colorimetric sensors with microfluidics has emerged as a promising approach for detecting various sweat analytes. This report demonstrates a fabric-based, skin-mounted microfluidic wearable device for continuous, real-time electrochemical pH monitoring and colorimetric chloride estimation in sweat. The pH sensor integrated into the microfluidics, utilizing electrodeposited polyaniline (PANI) on carbon cloth (CC), exhibits a significant sensitivity of 75.15 mV/pH, within a pH range of 2–9, closely matching Nernstian behavior. The sensor exhibited excellent repeatability, selectivity for target ions, and stretchability, with accuracy confirmed through a commercial pH meter. Additionally, the colorimetric sweat chloride concentration was estimated using image processing, covering a wide linear range of 10–125 mM with a detection limit of 8.3 mM in real-time. An array of skin-mounted microfluidic devices integrated with a miniaturized circuit module for smartphone readout successfully monitored sweat pH, chloride levels, and local sweat loss/rate in volunteers during their physical activity. This sustainable and non-invasive sensor demonstrates reliability and unveils promising applications in real-time human health monitoring systems.

1. Introduction

Flexible and wearable biosensors have received great attention in health sectors owing to their competence to provide non-invasive, continuous, and real-time monitoring of an individual's physiological status through biological fluids such as sweat, saliva, tears, and urine [1,2]. Among these fluids, sweat is an optimal surrogate diagnostic fluid because of its abundance of various metabolic and physiological biomarkers associated with metabolic activities, hydration status, diabetes, cystic fibrosis, and drug-related investigations [3–5].

Among various indicators, sweat pH is a crucial metric for assessing metabolism and homeostasis by measuring the concentration of hydrogen ions, which are essential for maintaining vital physiological functions [6]. Accurate detection of sweat pH is profoundly beneficial for the early detection of a range of diseases, including kidney dysfunction, diabetes, and skin conditions [7]. For instance, patients with type 2 diabetes mellitus often show lower pH values, while those with cystic fibrosis tend to have higher alkaline sweat (up to pH 9) compared to healthy individuals (with a pH range of 4.5–6.5). Similarly,

when a wound becomes infected, its pH typically ranges from 7 to 8.5 due to the presence of bacterial colonies and enzymes [8]. Moreover, the pH level of sweat is intricately connected to our skin. Thus, the fluctuations in sweat pH can serve as indicators of skin diseases such as atopic dermatitis, ichthyosis, and fungal infections [9,10].

Cystic fibrosis (CF) is an inherited, chronic condition that affects the lungs and digestive system, verge to a shortened life expectancy of 30–40 years, emphasizing the vital importance of early diagnosis [11,12]. In clinical practice, sweat chloride levels are recognized as the gold standard for diagnosing CF. Patients with CF exhibit impaired chloride transport, resulting in elevated sweat chloride levels. This is caused by defects in the cystic fibrosis transmembrane conductance regulator (CFTR) chloride channel. Chloride concentration levels in sweat below 40 mM are classified as normal, whereas levels exceeding 60 mM are indicative of CF. When concentrations fall between 40 and 60 mM, there may be a potential risk for CF. Consequently, the quantification of sweat chloride serves as a vital diagnostic tool for identifying CF [13,14]. Furthermore, the monitoring of sweat rate/loss enables customized and timely responses for athletes, military

* Corresponding author.

E-mail address: cji@ajou.ac.kr (J. Choi).

<https://doi.org/10.1016/j.cej.2024.158979>

Received 14 June 2024; Received in revised form 9 November 2024; Accepted 24 December 2024

Available online 25 December 2024

1385-8947/© 2024 Elsevier B.V. All rights are reserved, including those for text and data mining, AI training, and similar technologies.

personnel, and medical dark practitioners in clinical settings, intending to avert potential dehydration, hyperthermia, and heat-related illnesses [15,16].

Electrochemical techniques play a pivotal role [5,17,18] in wearable sweat sensors, facilitating the continuous monitoring of distinct sweat biomarkers and metabolites such as pH, glucose, lactate, potassium, sodium, and cortisol [19–23]. These techniques efficiently convert the analyte concentration into electrochemical signals. Lately, researchers have focused on developing wearable devices that integrate tattoos, wristbands, and textile-based sensors as alternatives for plastics and silicon materials [2,24]. Conductive fabrics have recently emerged as a promising alternative to the aforementioned substrates, offering comfort, flexibility, affordability, and high mechanical strength [25–27]. Carbon cloth (CC), a well-known conductive fabric, has recently gained widespread use in electroanalytical chemistry and materials science because of its intrinsic carrier mobility, strong mechanical properties, environmental stability, and affordability. The network structure functions as a supporting matrix that integrates different functional nanomaterials, increasing the surface area available for electrocatalytic reactions. This configuration enhances sensitivity and allows the device to bend and stretch, ultimately advancing its overall sensing performance [28]. Health monitoring wearable systems can integrate various flexible sensor components within textile fibers, microfluidics, elastic bands, or directly on the skin. This innovative approach in wearable technology enables flexibility in maintaining continuous and close contact with the human body [29].

Zhao et al. developed a wearable band made from hydrophobic-treated cotton fabric with embroidered thread for sweat collection and monitoring. However, low analyte concentrations, evaporation, and contamination during sampling can cause discrepancies in measurements, and many collection layers do not support directional sweat transport, hindering continuous monitoring [30]. Hence, a primary challenge with wearable fabric-based sweat sensors is developing a sensing element that can maintain consistent contact with the skin continuously [31,32]. In addition, continuous sweat analysis faces several significant challenges, such as sweat evaporation, uneven sweat distribution across the transducer surface, varying sweat volumes, chemical interferences, dilution effects, and mixing of sweat from different time intervals, leading to potential carryover effects. Mechanical movement can also induce friction between the sensing element and the skin's surface, potentially damaging sensitive sensor components [33]. Thus, efficient collection and accurate detection of biomarkers in sweat are crucial aspects of wearable sweat sensors.

To mitigate these issues, microfluidic technology is employed for efficient and continuous sweat sampling, enabling electrochemical and colorimetric detection of sweat pH and chloride concentrations. The micro-sized channels enable rapid sampling, high flow rates, and efficient transmission across the detector surface, effectively preventing sweat evaporation and external contamination, even with small sample volumes. Further, the microfluidic channels avert sweat re-absorption back into the skin, enhancing the accuracy and reliability of wearable sensors [34]. Additionally, integrating textile-based sensor electrodes into microfluidics offers greater flexibility and comfort compared to conventional sensor design. The combined electrochemical and colorimetric detection of multiple analytes in sweat facilitates the analysis of various biomarkers from a single sample collected at one physical location. Given the importance of pH and chloride and their interrelation in sweat, there is a strong need for a fully integrated wearable platform that can monitor these parameters simultaneously and provide real-time feedback during everyday activities.

This paper presents a fabric-based, flexible microfluidic wearable sensor designed to collect sweat and perform dual functions: continuous electrochemical detection of pH and colorimetric analysis of chloride concentration in sweat. The sensor utilizes the PANI-deposited functionalized CC (FCC) as a selective pH working electrode (WE), coupled with a polyvinyl butyral membrane coated Ag/AgCl@CC as the

reference electrode (RE). The pH sensor quantitatively measured the pH levels ranging from 2 to 9 in sweat buffer solutions, demonstrating Nernstian behavior with a sensitivity of 75.15 mV/pH. To facilitate real-time sweat monitoring, the pH sensor is integrated with a microfluidic device, coupled with a reusable flexible printed circuit board (PCB) containing signal transduction, conditioning, processing, and wireless transmission for smartphone readout. Furthermore, the colorimetric estimation of chloride concentrations and localized sweat loss/rate performed by this sensor system are closely associated with dehydration, making them valuable screening biomarkers for CF. Human studies were performed to confirm that the microfluidic wearable system can continuously monitor pH, chloride concentration, and sweat loss/rate in subjects during exercise, facilitating a broad spectrum of personalized diagnostic and physiological monitoring applications.

2. Materials and methods

2.1. Materials

Bleached and scoured CC was purchased from Nara Cell-tech, Seoul, South Korea. Aniline, sulfuric acid, hydrogen chloride, sodium hydroxide, polyvinyl butyral, potassium hydrogen phthalate, tris(hydroxymethyl)aminomethane, potassium dihydrogen phosphate, borax, sodium chloride, calcium chloride, potassium chloride, magnesium chloride, D(+)-glucose, lactic acid, urea, uric acid, triglycerides and ammonium chloride were sourced from Sigma-Aldrich. All reagents were used without further purification. The ultrapure DI water (specific resistance 18 M Ω /cm) was employed throughout experiments. The pH buffer solution was formulated by combining 5 mM of potassium hydrogen phthalate, potassium dihydrogen phosphate, and tris (hydroxymethyl)aminomethane, alongside 2.5 mM of borax, and 100 mM of sodium chloride. All electrochemical experiments were conducted using an electrochemical workstation (PalmSens4, Netherlands).

2.2. Preparation of PANI onto CC

Before the electrodeposition of PANI, the CC underwent ultrasonic cleaning with acetone and ethanol for 15 min. Subsequently, it was immersed into a solution consisting of a 1:3 ratio of HNO₃ and H₂SO₄ for 3 h at 70 °C to endure chemical functionalization for the introduction of surface carboxyl groups. Following this, the FCC was rinsed with DI water until neutralization and then dried at 60 °C under vacuum overnight.

To fabricate the pH sensing electrode, the chronoamperometric technique was employed in a mixed solution of 0.5 M H₂SO₄ and 0.2 M aniline at 0.7 V for 3 min. The electrodeposition potential was controlled at 0.6, 0.7, and 0.8 V vs. Ag/AgCl respectively to attain a uniform coating of PANI on the FCC surface. The sample was retrieved, subjected to three rinses with DI water, and subsequently left to dry at 60 °C overnight. [35] This process was carried out within a conventional three-electrode system, utilizing a PalmSens4 electrochemical workstation. The FCC served as the WE, while the Pt wire and Ag/AgCl functioned as the counter and reference electrodes, respectively.

2.3. Preparation of Ag/AgCl reference electrodes

In potentiometric sensors, the RE indeed remained insensitive to fluctuations in chloride ion (Cl⁻) concentration. This was typically achieved by introducing a saturated polymeric membrane with chloride salt onto the Ag/AgCl coating. To construct a flexible CC-based Ag/AgCl RE, the CC underwent two dips in Ag/AgCl ink, followed by curing at 90 °C after each coating for 20 min. Afterward, the Ag/AgCl@CC was submerged into a reference membrane solution for 60 s and allowed to dry overnight at room temperature. In the preparation of the reference membrane, 78 mg of polyvinyl butyral (PVB) and 50 mg of NaCl were dissolved in methanol (1 mL), under vigorous stirring to ensure

uniformity [36,37]. Drop-casting the PVB/NaCl membrane onto the Ag/AgCl layer was commonly employed for wearable potentiometric sensors. Furthermore, the FESEM micrographs and comprehensive EDS analysis of Ag/AgCl@CC were depicted in Fig. S1.

2.4. Materials characterization

The morphology and elemental composition of the prepared materials were evaluated using a Field emission scanning electron microscope (FESEM, JEOL-JSM-7900F, Japan) at an accelerating voltage of 10 kV, equipped with an Energy Dispersive X-ray spectrometer (EDS). X-ray diffraction (XRD, Rigaku Ultima IV, Japan), Raman spectroscopy (HORIBA, LabRam with an excitation laser of 514 nm), and X-ray photoelectron spectroscopy (XPS, Multilab 2000, UK) were utilized to examine the crystal structure, chemical composition, and surface chemistry of both the bare and PANI/FCC materials. The contact angle measurements were conducted using a KRÜSS DSA 20E, equipped with a CCD camera module to monitor the wettability of the modified CC fabric for electrochemical sensing applications. The air permeability of pristine and modified CC was measured using an automatic air permeability tester (FX3300-IV, TEXTTEST Instruments, Switzerland) in accordance with the ASTM D737:2018 standard. Further, the tensile strength of pristine CC and PANI@CC was tested using a universal testing machine (UTM, Zwick Roell, USA) following ASTM standard D4851. AutoCAD 2024 software was used to design custom-size CC for both WE and RE (working area of 4 mm in diameter). Subsequently, the infrared CO₂ laser from Oxford Laser Systems (United Kingdom) was employed to cut the CC, aiding optimized parameters such as a speed of 10 mm/s and a power of 50 W.

2.5. Fabrication of the microfluidic module

Fig. 1a illustrates a schematic representation of the different layers of the microfluidic sensing device. A standard soft lithography technique was utilized to fabricate microfluidic PDMS channels [38,39]. The fabrication began with the formation of a mold from a 4-inch silicon wafer pattern. Specifically, the photoresist KMPR1010 was spin-coated onto a silicon wafer (1 mm thick) at 3000 rpm for 30 s and then baked on a hot plate at 110 °C for 5 min. It was subsequently exposed to UV irradiance at 200 mJ/m² for 10 s and developed using SU-8 developer (Kayaku Advanced Materials, USA). Afterward, deep reactive-ion etching (polymethylmethacrylate coating; STS Pegasus ICP-DRIE; SPTS

Technologies Ltd) was employed to remove the exposed silicon to a specified depth of around 600 μm. During the etching process, a thin layer of fluorinated polymer (CFn) formed on the surface, facilitating the release from the mold. After the fabrication of this mold, poly(methyl methacrylate) (PMMA) was spin-coated onto the patterned silicon mold and then baked at 110 °C for 3 min. To complete the fabrication of the proposed microfluidic device, the various thickness PDMS layers were prepared on the mold as described in the following steps.

The polydimethylsiloxane (PDMS) base, curing agent (Sylgard 184, Dow Corning), and white silicone dye (Silicone Pig, Smooth-On) were combined in a weight ratio of 10:1:1 and placed into a vacuum chamber for 30 min to eliminate any air bubbles. The degassed PDMS mixture was then spin-coated onto the developed mold at 200 rpm for 30 s, followed by baking at 130 °C for 3 min to yield a 600-μm-thick, soft, white microfluidic structure. A mechanical punch tool was employed to define 1-mm-diameter sweat solution inlet holes for both the rectangular electrochemical and colorimetric sensor chambers [40].

Additional PDMS layers were prepared by pouring the PDMS base and curing agent (in a 10:1 ratio) mixture onto a PMMA-coated silicon wafer, followed by spin-coated at 400 rpm. The curing process at 130 °C for 5 min produced 200 μm-thick uniform, transparent top and bottom layers for the microfluidic platform. A CO₂ laser (Universal Laser Systems, AZ, USA) was used to define sweat inlet holes in a skin-adhesive membrane (PC2723U, Scapa Healthcare).

The assembly of the microfluidic device involved placing the pH sensor electrodes and the colorimetric assays into their designated chambers. The sticky side of the capping layer was then applied over the top and bottom of the microfluidic patch. Using a handheld corona generator to treat the skin-adhesive membrane, the color reference marker film, and the microfluidic platform resulted in hydrophilic surfaces. This facilitated the efficient bonding of layers to be stacked to complete the fabrication process of the microfluidic device. The detailed design of a microfluidic sweat collection system for the epidermal electrochemical sensor was given in Fig. 1 and supplementary information.

2.6. Development of colorimetric assays for chloride sensing

The solution for the colorimetric chloride assay was prepared by dispersing 50 mg of silver chlorinate (MP Biomedicals, CA, USA) in 200 mL of a 2 wt% polyhydroxyethyl methacrylate (pHEMA) (Sigma-Aldrich, MO, USA) solution [32,38]. Then, 5 μL of this chloride assay

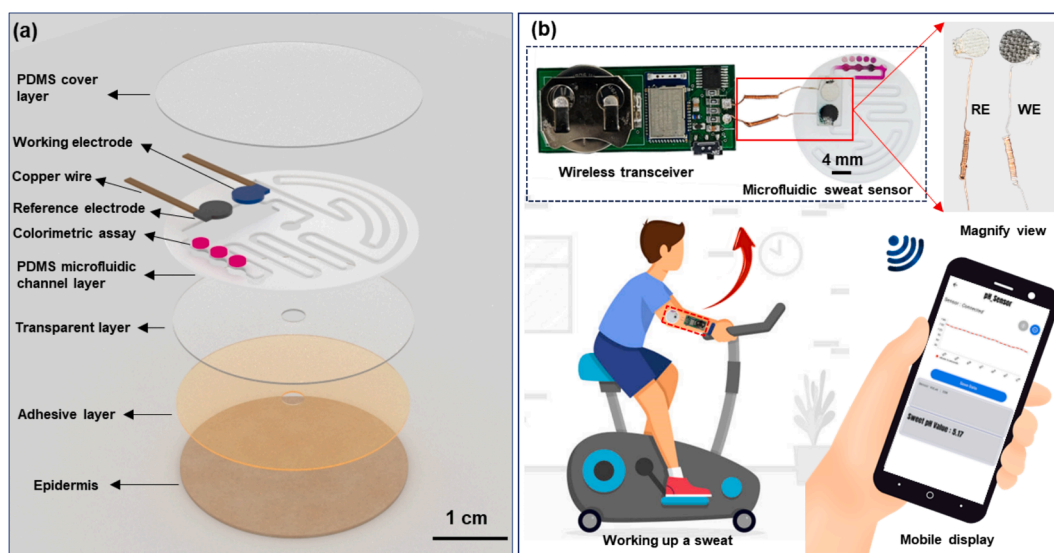


Fig. 1. The outline of the wearable microfluidic sweat sensor design. (a) The schematic presents the exploded view of the layers and components of the microfluidic system and (b) the preparation emphasizing a fully integrated wearable microfluidic sensing system worn by a subject, along with a mobile application.

cocktail was drop-cast into the microfluidic chambers specifically designated for chloride sensing. The three posts located within the reservoirs serve a dual purpose: they prevented mechanical collapse and trapped air bubbles during the flow of sweat, as shown in Fig. 1a. The calibration plot for chloride concentrations was generated by exposing chloride assays to standard NaCl solutions within a concentration range of 10–125 mM. Images of the assays were captured using a smartphone camera (Samsung S20 Ultra, 5G), and further analysis was conducted using Photoshop (Adobe Systems, CA, USA) with optimized parameters of ISO aperture and shutter speed.

A color laser printer (C454 PS; Konica Minolta, Tokyo, Japan) was used to create color reference markers on photo sheets. The laser-cut (Oxford Laser Systems, UK) color reference markers (2 mm in diameter) were placed adjacent to the assay chambers, and the images were captured using a smartphone (Samsung S20 Ultra, 5G). This setup enabled the comparison of color values (RGB color model and lightness value from Lab color space for chloride assay) of the reference markers with the assays. In the chloride analysis design, a lengthy (1 cm) meandering microchannel was integrated to ensure consistent color development, unaffected by varying sweat rates, even at higher levels.

2.7. Fabrication of wireless transceivers

The fabricated microfluidic wearable sensor was impeccably integrated with an electronics module comprising a microcontroller, front-end circuit, battery, and switch, facilitating continuous monitoring of sweat pH. For device operation and data transmission, we utilized the MDBT42Q-512KV2 Bluetooth Low Energy (BLE) module from Raytac Corporation, Taiwan, which features a Nordic Semiconductor nRF52832 System on Chip (SoC). This SoC includes a multi-protocol 2.4 GHz radio, a 32-bit ARM Cortex-M4F processor, 512 kB of flash memory, 64kB of RAM, 32 GPIOs, and interfaces such as SPI, UART, I2C, I2S, PWM, ADC, and NFC. The module operates within a supply voltage range of 1.7 V–3.6 V, consuming ~ 5.4 mA of current during reception, ~ 5.3 mA during transmission, and ~ 1.9 μ A in sleep mode.

In the front end, we employed a voltage follower, and a differential circuit using an operational amplifier (AD8608, Analog Devices Inc., USA) to measure the potential difference between the fabric-based WE and RE. This amplifier offers an ultra-low offset voltage (<65 μ V), minimal input bias current (<1 pA), low noise (8 nV/ $\sqrt{\text{Hz}}$), and a broad signal bandwidth (10 MHz). Additionally, it features stable unity gain with rail-to-rail operation, ensuring precise measurements across a broad range of signals.

The differential amplifier's output signal is sampled every second by the on-chip Analog-to-Digital Converter (ADC) integrated within the SoC. The digitized data is wirelessly transmitted to a smartphone via BLE. A custom smartphone application was also developed using the Android Studio IDE to facilitate real-time continuous data monitoring. The application provides graphical representations of the data and displays the associated sweat pH value. A two-layer printed circuit board (area: 22 mm \times 48 mm) was designed using Autodesk EAGLE software and manufactured using standard PCB technology. The device was powered by a 3 V Panasonic CR2032 lithium battery (225 mAh), and a miniaturized AYZ series slide switch (C&K Components) is used for power control, ensuring efficient user-friendly management. A coiled copper wire was used to establish the contact between the fabric-based electrodes in the microfluidics and the custom-made PCBs. This wire design allows the system to bend and conform to various shapes without compromising power transmission or efficiency, ensuring flexibility and durability in wearable applications.

Fig. 1b depicts the flexible microfluidic sensing device impeccably integrated into human skin, enabling real-time collection of sweat pH and wireless monitoring via a mobile device. The block and circuit diagram of the electronics circuit module are provided in the Supporting information (Fig. S2).

2.8. On-body sweat sensing

Four healthy adults, who provided their consent, participated as volunteers in the on-body assessment of the microfluidic wearable sweat sensor. The mounting locations (forearm, forehead, chest, and back) were thoroughly cleaned using wet wipes and an alcohol swab before attaching the biodegradable microfluidic devices. The volunteers were instructed to ride a stationary cycle for ~ 40 to 50 min at room temperature and ~ 30 % relative humidity. After background calibration, the real-time sweat pH value was continuously measured via a PCB board enabling electrochemical detection with data acquisition by the smartphone reader. During the human trials, digital images were taken using smartphone cameras at regular intervals for calculating sweat loss/rate and conducting colorimetric analyses. The total sweat loss from the specific region was determined using image-based sweat volume analysis, serving as the benchmark to evaluate the accuracy of the developed sensor. Additionally, the CIELAB and RGB color values from the microreservoirs were obtained from the images corresponding to chloride concentrations.

3. Results and discussion

3.1. Structural, morphological, and compositional analysis of CC and PANI/CC

A schematic illustration demonstrating the acid treatment of CC and the PANI deposition onto FCC is provided in Fig. 2a, to elucidate the derivatization process. The FESEM analysis was performed to examine the microstructure of bare, FCC, and PANI/FCC. Fig. 2b reveals that the flexible and robust pristine CC exhibits a woven structure with a smooth surface, featuring a diameter of ~ 10 μ m. After exposure to the chemical treatment, the functionalized CC demonstrates relatively rough surfaces compared to bare CC, as shown in Fig. 2(c and d). The surface wettability and electronic conductivity enhanced, thereby introducing chemically active sites into the CC network. The FESEM images of PANI/FCC displayed in Fig. 2(e–g) reveal the uniform network-like morphology of PANI nanostructures on the FCC skeleton, facilitated the electrodeposition process, demonstrated a strong adhesive force between the PANI and FCC matrices. The network-like PANI structure on the FCC surface was formed through the in-situ polymerization of aniline monomers in an H₂SO₄ aqueous solution under optimized parameters including aniline concentration (0.1 M and 0.2 M) and the applied potential (0.6 V–0.8 V) (Fig. S3). As a result, the surface displayed a positive charge of PANI resulting from doping with H₂SO₄, thereby impeding the adsorption of protonated aniline. The chemical functionalization of CC can enhance faster nucleation and growth kinetics.

The FESEM micrographs of the Ag/AgCl-coated CC display a granular surface with diverse grain sizes (~ 100 nm) and stacked layers of grains as illustrated in Fig. S1. Furthermore, at higher magnifications, pores resembling microchannels are evident on the outer layers (Fig. S1d), enabling the transport of ions through the film. In Fig. S1 (e–i), the EDS spectra and mapping display the elemental composition and uniform distribution of Ag and Cl along with C and O on the CC surfaces.

The EDS analysis was utilized to investigate the purity and quantify the elements present in the bare and PANI/FCC. The EDS spectrum depicted in Fig. S4 confirmed that the electrodeposited PANI/FCC contained carbon (89.18 %), nitrogen (5.38 %), and oxygen (5.44 %), as compared to bare CC. The presence of a small amount of oxygen in the PANI/FCC indicates the formation of oxygen-containing hydroxyl and carboxyl groups on the PANI surface. Furthermore, the EDS elemental mapping shown in Fig. S4 illustrates consistent spatial distributions of C, N, and O without any self-aggregation.

The XRD was utilized to analyze the phase purity and structure of both CC and PANI/FCC. Fig. 3a presents the XRD spectra for CC, revealing two prominent peaks at approximately 25.8° and 42.9°,

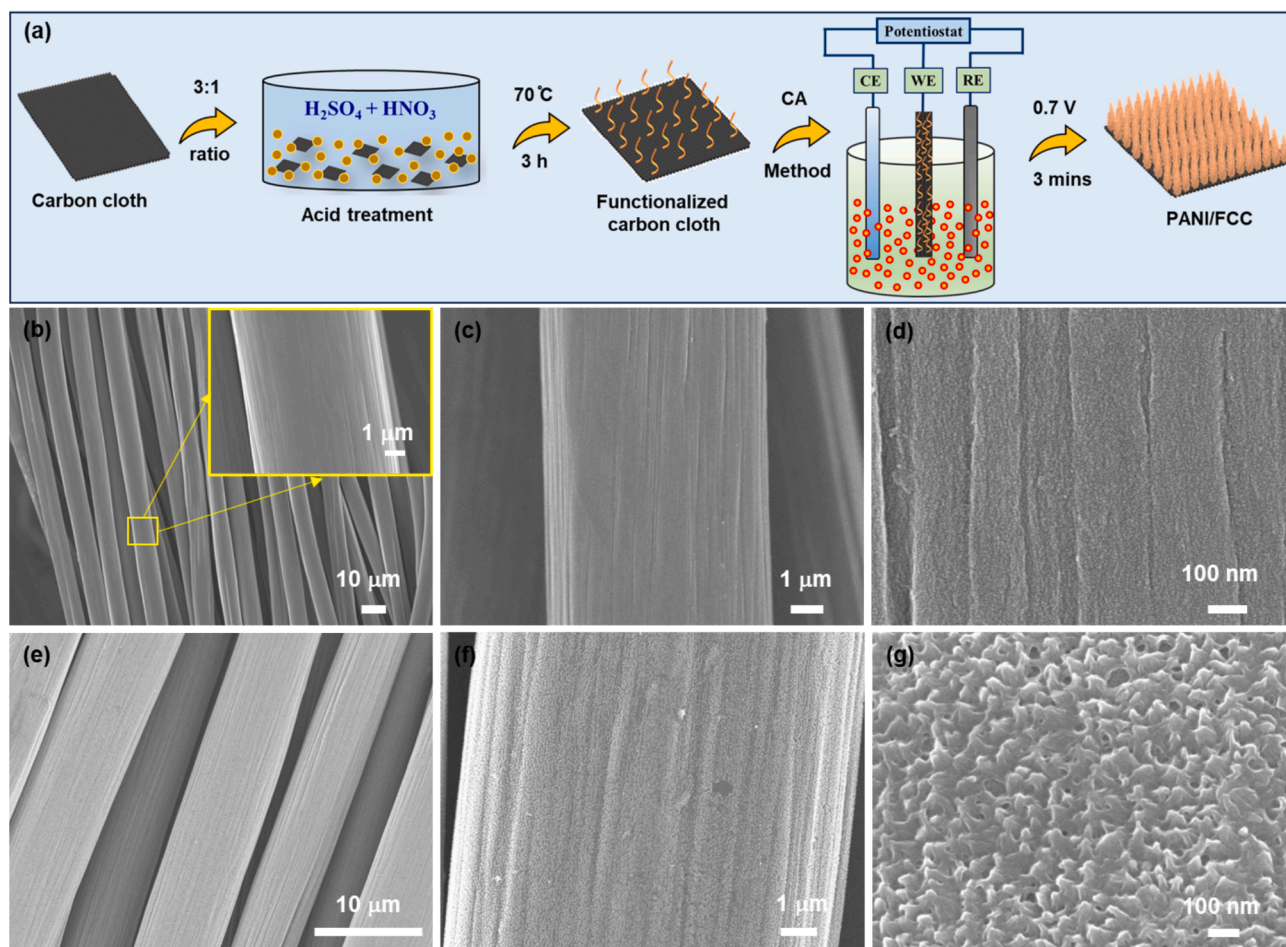


Fig. 2. Morphological characterization of bare and PANI/FCC. (a) Schematic representation of chemical treatment and PANI deposition on FCC using the chronoamperometry method. FESEM analysis of (b) bare CC, (c and d) FCC, and (e–g) PANI-integrated FCC.

corresponding to the (0 0 2) and (1 0 0) planes of graphite-like materials, respectively. The peaks observed for FCC correspond to its turbostratic carbon structure [41]. The broadness of these peaks suggests the low crystallinity of the FCC. The XRD pattern of PANI/FCC exhibits an amorphous nature, with peaks observed at 9.4° and 19.8° corresponding to reflections from the (0 0 1) and (0 2 0) planes, respectively. The prominent peak of the FCC is anticipated at around $2\theta = 25^\circ$, potentially coinciding with the PANI–FCC peak [42]. These outcomes indicate the successful synthesis of PANI in its emeraldine salt form onto CC. To further investigate the functional characteristics of the PANI/FCC, Raman spectral analysis was conducted, and the details are provided in Fig. S5.

Additionally, XPS analysis was utilized to investigate the diverse elemental compositions and surface features of pristine and PANI-coated fabric. Illustrated in the survey spectrum (Fig. 3b), the composite textile PANI/FCC predominantly comprises the elements C, O, and N. Indeed, the presence of N in FCC suggests its chemical environment, likely originating from the electrolyte used during the functionalization process. Following electrodeposition, the surface concentrations of C and O diminish while that of N increases, indicating successful integration of PANI onto FCC [42] depicted in Fig. 3c, the N 1s spectrum reveals three primary peaks around 398.2 eV, 399.4 eV, and 401.5 eV, representing quinonoid imine ($-NH=$), benzenoid amine ($-NH-$), and protonated (NH^+) functional groups, respectively. The $NH/(NH + NH^+)$ ratio of 1.02 suggests oxidized emeraldine in the electrodeposited PANI. The C1s spectrum of CC and PANI/FCC (Fig. 3d) has two distinguished peaks with binding energies of 284, and 286 eV, corresponding to graphitic carbon, and carboxyl groups, respectively. Notably, the C 1s XPS spectra

of CC and PANI/FCC exhibit two deconvoluted peaks, corresponding to aromatic C–C/C=C (284.49 eV) and C–N/C=N (285.45 eV) for CC, and aromatic C–C/C=C (284.66 eV) and C–N⁺/HO–C=O (286.57 eV) for PANI/FCC. This observation implies that the electrodeposition process facilitates the introduction of dopant ions into PANI chains on CC. Furthermore, the O1s XPS spectra of PANI/FCC are deconvoluted and fitted with two peaks at 531.44 and 532.6 eV, which is derived from quinone (C=O, C–OH), and chemisorbed oxygen species (Fig. 3e) [43,44]. These varied functional groups played a role in enhancing the interfacial interaction between PANI and carbon fibers, encompassing electrostatic interactions, hydrogen bonding, and π – π stacking.

The water contact angle (WCA) measurement, indicating the hydrophobic or hydrophilic nature of a material, is crucial for understanding sweat-wicking behavior for developing wearable biochemical sensors. The results obtained from WCA measurements for both bare and PANI/FCC are depicted in Fig. 3f. The bare CC surface exhibited superhydrophobic properties, with a contact angle exceeding 150° . Upon integrating PANI, the CC showed a notably accelerated wetting time, with water droplets promptly absorbed by the PANI/FCC structure. As illustrated in Fig. 3f, water spread rapidly on this hydrophilic PANI/FCC surface, resulting in a contact angle close to 10° . The increased hydrophilicity attributed to PANI is an important characteristic of wearable biosensors, as it facilitates easy absorption of sweat samples by the fabrics [45]. Furthermore, air permeability and adhesion strength are essential properties for evaluating the potential of fabric substrates in wearable sensor applications. As shown in Table S1, the air permeability of PANI@FCC increased compared to pristine CC (8 mm/s) due to the network-like structure of the deposited layer, which

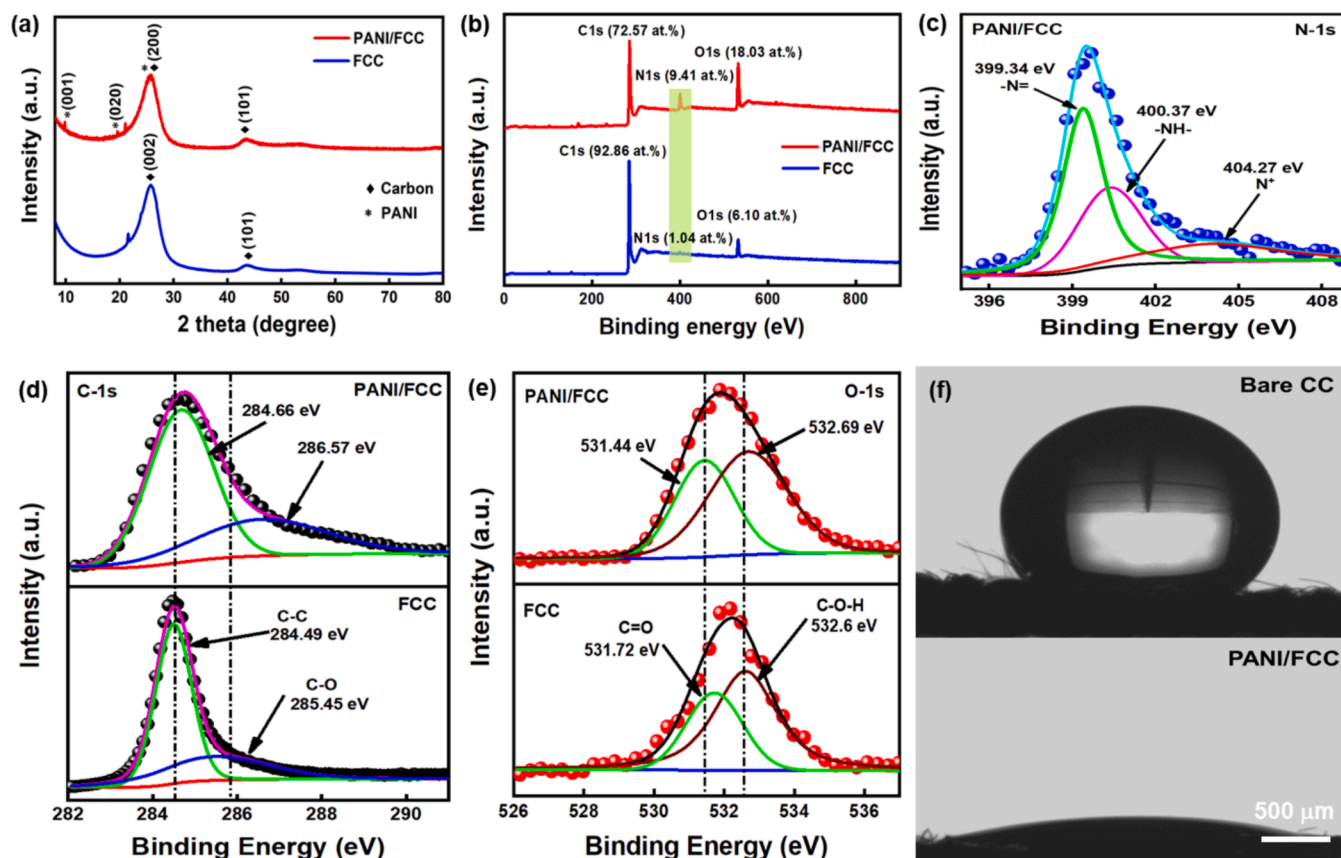


Fig. 3. Structural and surface analysis of pristine and PANI/FCC. (a) XRD, (b–e) XPS, and (f) wettability analysis of bare and PANI integrated CC.

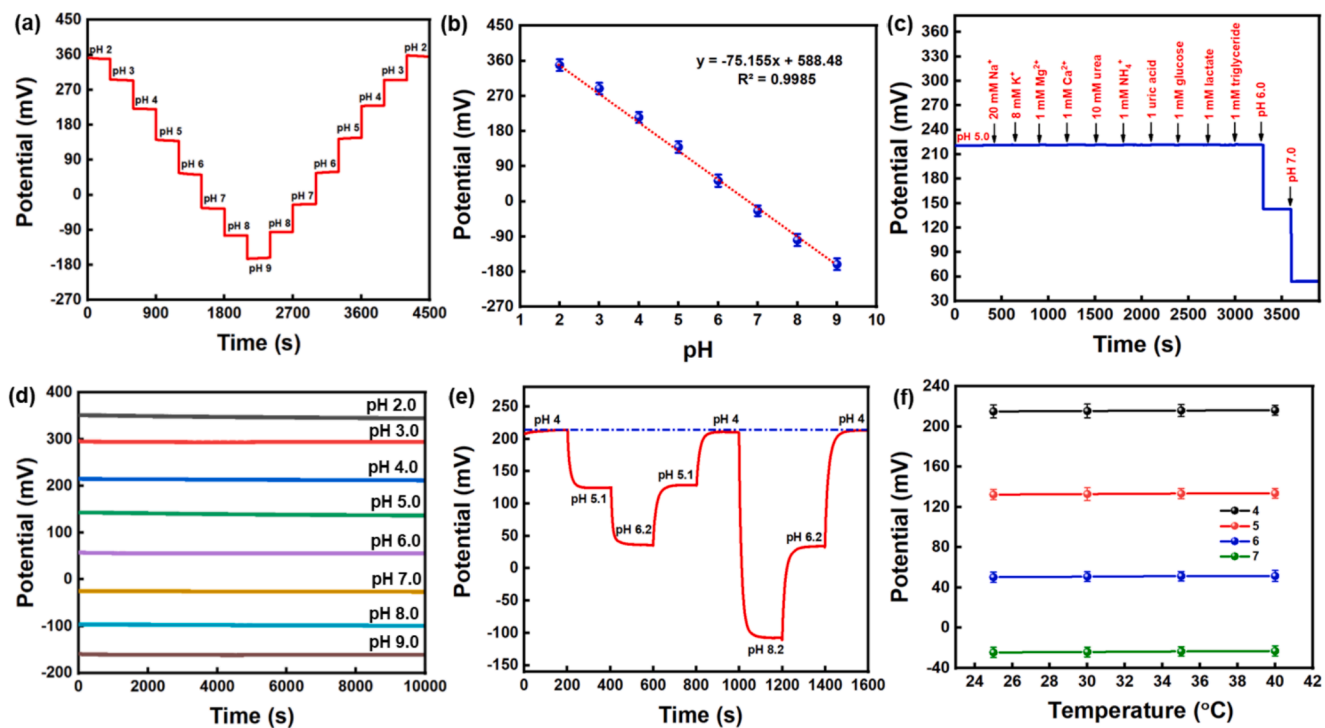


Fig. 4. Electrochemical analysis of pH sensors. (a) Sensitivity, (b) indicates a linear relationship between OCP and pH (c) selectivity, (d) long-term stability (e) repeatability, and (f) temperature effect fabricated pH sensor.

maintained good air permeability. The sensor reached a maximum air permeability of 166 mm/s at a pressure of 125 Pa. Results illustrate that the tensile strength of PANI@CC increased to 25.4 ± 0.6 MPa, compared to 12 ± 0.8 MPa for pristine CC. This enhancement is attributed to the chemical treatment and increased surface roughness from the network structure of PANI on CC.

3.2. Electrochemical performances of microfluidic pH sensor

The overall electrochemical performance of the fabric-based microfluidic pH sensors is assessed as depicted in Fig. 4. Due to its ease of fabrication, reproducibility, and biocompatibility, PANI is commonly employed for pH measurement in body fluids. This present study involved assembling the PANI/FCC and Ag/AgCl@CC to develop a flexible microfluidic pH sensor. Beforehand, the pH-sensing performance was tested by immersing the two electrodes into 1 mL of standard artificial sweat buffer solution spanning pH levels from 2 to 9, reflecting the typical pH of human sweat, in both ascending and descending order as proved in Fig. 4a. The open circuit potential (OCP) value consistently decreased with increasing pH, exhibiting an average slope of 75.15 mV/pH with an RSD of 1.0 % over full cycles from pH 2 to 9 in room temperature. Successive numerical fitting revealed a strong linear relationship between the potential with a sensitivity of 75.15 mV/pH ($R^2 = 0.998$), closely aligning with the theoretically predicted pH sensitivity based on the Nernst equation as illustrated in Fig. 4b [46]. The pH sensing mechanism of PANI is based on a reversible protonation and deprotonation process as shown in Fig. S6. The amine and imine groups in the emeraldine base (EB) can be protonated to form the conductive emeraldine salt (ES). This protonation-deprotonation cycle between EB and ES imparts pH sensitivity to PANI. The sensitivity of the PANI-based fabric sensor demonstrates a rapid response that corresponds to the gradient in sweat pH. Furthermore, the electrochemical characterization through CV and EIS analysis for CC, FCC, and PANI@FCC was carried out and is shown in Fig. S7. Further we have compared the highlights of the proposed sensor system with previously reports as illustrated in Table 1.

Fig. 4c illustrates the interference impact of various ions, including Ca^{2+} , Mg^{2+} , NH_4^+ , Na^+ , K^+ , glucose, lactate, urea, uric acid, and triglycerides. The fabric-based pH sensor demonstrates excellent pH selectivity, displaying no potential changes in the presence of these interfering ions, except for hydrogen ions.

Furthermore, pH sensor experiments were conducted following the integration of the sensor electrodes into the microfluidic device. A standard sweat buffer solution of 100 μL was injected into the microfluidic channel using a flow meter, and the long-term stability of the pH sensor was evaluated by measuring the OCP value for pH 2 to 9 over 10,000 s (Fig. 4d). No significant difference was observed in sensor performance with or without integration into the microfluidic channel. The results revealed an insignificant change in potential, with a value of <2 mV and a sensitivity of 75.15 mV/pH. This performance was found to exceed earlier claims regarding the stability of PANI as a pH-sensitive material.

Repeatability plays a vital role in the performance and reusability of pH sensors, especially considering their need to withstand prolonged exposure to fluctuating pH levels. To evaluate the fabric pH sensor's repeatability, its OCP responses were measured across a titrated cycle covering pH levels of 4, 5.1, 6.2, and 8.2. During the titration process, 1 M HCl or NaOH solution was added to the buffered solution to respectively decrease/increase its pH levels. As revealed in Fig. 4e, the reaction attains equilibrium immediately after the pH changes in the buffer solution, with a rapid response time of about 20 s. The prepared PANI-based pH sensor demonstrates rapid and reversible transitions across various buffer solutions, with the electrode returning to its initial OCP value even after exposure to an acidic (pH 4.0) buffer solution. This outcome ensured the excellent repeatability performance of the prepared sensor, indicating its potential for reusability. A significant

challenge in the quantitative analysis of body fluids is the impact of chloride ions (Cl^-) on solid-state RE (Ag/AgCl@CC). However, this challenge has been addressed with PVB-based Ag/AgCl@CC, which has shown exceptional relative stability. Overall, the examination outcomes indicate that the current pH sensors provide precise and reliable analysis capabilities.

As this system is intended for medical applications, it is essential to assess the microfluidic pH sensors at temperatures that align with physiological conditions. The human body maintains an internal temperature of $\sim 37^\circ\text{C}$, while the skin temperature typically varies between 25°C and 35°C , depending on environmental factors [47]. Fig. 4f illustrates the pH measurement results at different temperatures. The sensor exhibits a slight increase in sensitivity at elevated temperatures ($25\text{--}40^\circ\text{C}$) for pH levels between 4 and 7, consistent with the Nernstian theory. The sensor exhibits an average negligible variation of ± 2 mV in readings compared to measurements taken at room temperature. These minor errors are deemed acceptable for point-of-care/clinical applications, considering the robust output of our sensor. Long-term stability is essential for the practical use of a pH sensor. This fabric-based pH sensor was evaluated over 30 days, with Fig. S8 illustrating the sensor's sensitivity over time in various pH electrolyte solutions. The average variation in potential and slope was less than 6 mV and 1 mV/pH, respectively, with a relative standard deviation (RSD) below 1.8 % over 10 tests conducted during the 30 days, showing no consistent trend in potential shifts. The slope remained stable at approximately 75 ± 2 mV/pH. These results indicate that the fabricated PANI-based pH electrode demonstrates excellent stability for long-term pH measurement applications.

3.3. Reusability analysis of microfluidic wearable sensor

Biosensors should not only be efficient but also reusable. Reusability could effectively reduce the cost of fabric sensor electrodes [48], and a recovery experiment was carried out to test the reusability of the CC-based microfluidic pH sensor. The assembled wearable sweat analysis system comprises three key components: the microfluidic device, electrochemical sensing electrodes, and a custom-made PCB. In this setup, the microfluidic channel layer is a disposable component, while the pH-sensing electrodes and PCB are reusable. To ensure reusability, the sweat buffer solution was infused into the microfluidic sensing system with pH sensor electrodes (device #1), where the pH was measured at 5.22 over time. Then, the system (device #1) was disassembled, the microfluidic channel was disposed, and the pH sensing electrodes and PCB were integrated with a new microfluidic chamber (device #2). Testing with the same buffer solution showed a pH of 5.17, indicating that the pH response remained stable in the two devices ensuring the reusability of the sensing electrodes and PCB as depicted in Fig. S9 and S10. Furthermore, the microfluidic pH sensor was integrated with PCB and measured the OCP value for pH 5 and pH 6 solutions over fabric sensor repetitions, as depicted in Fig. S11. The results were displayed on a smartphone, demonstrating negligible potential drift. Hence, the CC fabric sensor possesses excellent reusability and economical durability to detect sweat pH in practical applications.

Moreover, achieving efficient operation as a wearable epidermal device necessitates the flexibility and stretchability of the microfluidic electrochemical sensing system to conform for skin mounting. Therefore, we investigated the effect of mechanical strain permutations on the device's integrity over repeated cycles. The physical appearance and electrode properties of the microfluidic platform remained unchanged after subjecting it to stretching, bending, and twisting as displayed in Fig. S12. The device's physical integrity and resilience, along with its custom-made PCB, were further validated through repeated cycles of bending, with no observable changes noted (Figs. S12 and S13). Additionally, the artificial sweat solution was infused into the microfluidic sensing device, which was attached to the volunteer's forearm. The pH was monitored using a smartphone every two hours throughout the day,

Table 1
Comparison table to highlight our results with previous findings.

Materials	Preparation method	Transduction mechanism	pH range	Response time	Sensitivity	Characterization Solution	Ref.
PANI on polymer-coated commercial paper	CV	Potentiometric	4–10	<10	50 mV/pH	Buffer	[52]
Iridium oxide film on Nylon based fabric	CV	Potentiometric	4–8	–	47.54 mV/pH	Buffer	[47]
Graphite-polyurethane composite on cellulose-polyester blend cloth	CV	Potentiometric	6–9	–	4 mV/pH	Buffer	[52]
PANI on gold fibers woven into a textile matrix	CV	Potentiometric	4–8	–	60.6 mV/pH	Buffer/artificial sweat	[53]
PEDOT:BTB on polyester thread	CV	Electrochemically gated	–	–	13 ± 10^{-3} pH	Buffer/real sweat	[54]
Laser-scribed Pt NPs nanostructured graphene	CV	Potentiometric	4–8	–	72.4 mV/pH	Buffer/real sweat	[55]
PANI on Polyethylene terephthalate	CV	Potentiometric	4–8	–	59.99 mV/pH	Buffer/real sweat	[56]
F-Ti ₃ C ₂ Tx/PANI on PET substrate	CV	Potentiometric	1–11	–	41.91 mV/pH	Buffer/real sweat	[57]
Au-PANI on PET substrate	CV	Potentiometric	4–7	–	62.5 mV/pH	McIlvaine's buffer/sweat	[58]
Iridium oxide on screen printed electrode in paper-based microfluidics	CV	Potentiometric	4–7	–	80 mV/pH	Buffer/real sweat	[59]
PANI film on the ternary composite electrode	CV	Potentiometric	3–7.4	–	63.96 mV/pH	Buffer/real sweat	[60]
PANI/CNT nanocomposites on CNT-AuNS electrodes	CV	Potentiometric	4–8	–	71.44 mV/pH	Buffer/real sweat	[61]
PANI on flexible interdigital gold electrodes	CA	Potentiometric	4–9	–	69.3 mV/pH	Buffer/artificial sweat	[62]
PANI on tattoo-based ion-selective electrodes	CV	Potentiometric	4–10	12	50 mV/pH	Buffer	[63]
PANI on CC	CA	Potentiometric	2–9	<10	75.15 mV/pH	Buffer/real sweat	This work

as shown in Fig. S14. These advantageous mechanical features enable its easy application as a continuous on-body sweat analyte monitoring device, without operational functional loss.

3.4. Quantitative colorimetric estimation of chloride concentration

As previously mentioned, an elevated concentration of chloride in sweat serves as a well-established marker for CF. The dimensions of the microfluidic network were customized to precisely measure the chloride concentrations. Antecedently, Fig. 5a displays an optical image of the microfluidic device filled with a NaCl solution via a syringe infusion pump (KdScientific, Legato 200) operating at a volumetric rate of 1 $\mu\text{L}/\text{min}$. It's noteworthy that the first column of the microfluidic channel was filled within 12 min, with the entire microfluidic channel taking ~ 40 min to fill. Silver chlorinates immobilized in a pHEMA framework solution serve as the colorimetric assay for chloride measurement in sweat. Upon interaction with chloride ions in sweat, it produces purple-colored ions. The porous hydrogel structure of pHEMA effectively traps the opaque white precipitates of AgCl, which formed during the reaction as depicted in Fig. S15. This outcome prevents the migration of silver

particulates during the flow of sweat in the microfluidic channel, thus eliminating their influence on color extraction. This leads to a considerable decrement in the RGB color levels and results in a dark purple color, as the concentration of chloride ions increases. Also, the lightness (L) level in the Lab color space serves as a representative metric for defining the color intensity of the assay under ambient lighting conditions. The color density produced is directly proportional to the concentration of chloride (10–125 mM) in sweat as shown in Fig. 5b. Colorimetric sweat sensors primarily operate through chemochromic mechanisms (Fig. S15), where ions form colored complexes by binding with complex ligands. The results from five consecutive colorimetric experiments ($n = 5$) are represented by the error bars and the corresponding results are provided in Fig. S16. The developed chloride sensor demonstrated a strong correlation coefficient of 0.98, with a limit of detection of 8.3 mM, calculated using standard deviation and slope values. Additionally, the color development of the chloride sensor corresponding to flow rates ranging from 0.5 $\mu\text{L}/\text{min}$ to 3.0 $\mu\text{L}/\text{min}$ is shown in Fig. S17. It is evident that the RGB and lightness values are not affected by the flow rates, which is consistent with previous reports [37].

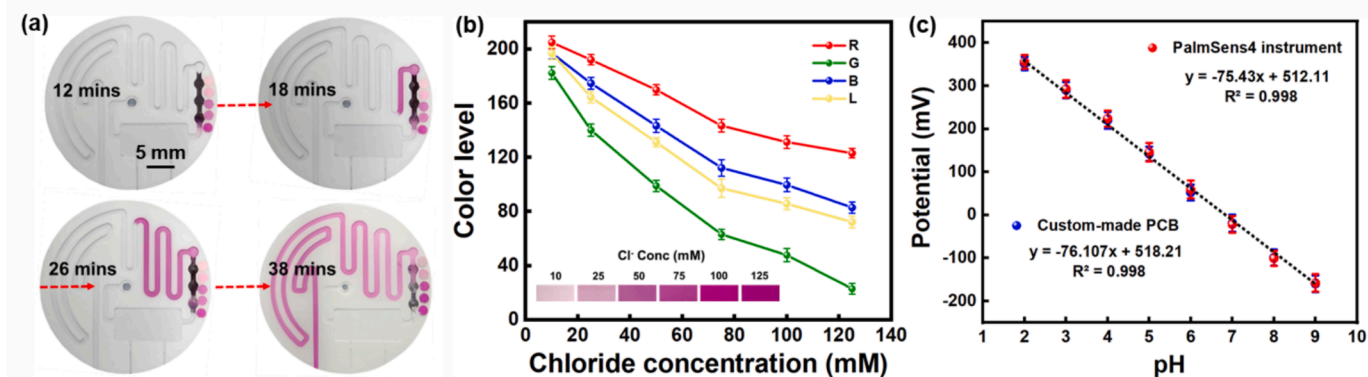


Fig. 5. Colorimetric analysis and device comparison. (a) Visual representations of the microfluidic sweat sensor filling over time, (b) Optical images illustrating the color development of the colorimetric assay in micro reservoirs to chloride concentration, and (c) A comparative linear graph depicting the sensitivity of pH 4–7 for both the PalmSens and the custom-made PCB.

To assess the selectivity profile of the chloride sensor, we examined a fixed 50 mM concentration of chloride salts with different cation species found in sweat, including Mg^{2+} (1 mM), K^+ (8 mM), Ca^{2+} (1 mM), and glucose (1 mM). The change in color intensity after the addition of these ionic solutions in the microfluidic device was investigated at a flow rate of 1 $\mu\text{L}/\text{min}$ (Fig. S18). No change in signal intensity was observed, indicating the sensor's tolerance towards the subjective ions [49]. Consequently, this proposed sensor demonstrates good selectivity, making it suitable for real-time sample analysis. Additionally, the shelf life of the chloride chemical assays was studied over a 30-day period, with the assays stored at 20 °C and 40 % relative humidity, as shown in Fig. S19.

The reliability of custom-made potentiostat in detecting sweat pH through the defined measurements was validated from the slope values of commercial PalmSens devices. [50]. Fig. 5c demonstrates the theoretically expected linear relationship between the potential and solution pH. The calibration curve for the sweat buffer solution ranging from pH 2 to 9 was acquired using the commercial potentiostat, exhibiting a sensitivity of 75.43 mV/pH, whereas our custom-made PCB demonstrated a sensitivity of 76.10 mV/pH. The resulting potential values obtained from both the potentiostat devices (Fig. 5c) comply with each other, confirming the reliability of our device over 98 %.

Following the completion of the ex-situ sweat analysis, we proceeded to conduct the real-time on-body evaluation of human sweat using the wearable microfluidic sensing system. By utilizing medical-grade skin adhesive tape, the sensor system could be securely affixed to the skin, even under mechanical bending. To maintain consistent skin contact and mitigate potential damage from mechanical movement, we employed highly flexible, biocompatible materials, enhanced sensor designs to minimize movement artifacts, and advanced medical adhesives for secure, long-term contact. Additionally, using coiled copper wire for electrode connections in microfluidics and custom-made PCBs improves flexibility, strength, and durability, making it suitable for applications requiring frequent bending and extended usability. Positioned at various body locations including the forearm, forehead, chest, and back (refer to Fig. 6), the system continuously collected sweat samples from the glands beneath the inlet of the microfluidic device. Fig. 6 portrays a subject wearing a comprehensive pH sensing system on the body, facilitating dynamic analysis of sweat pH values during cycling activities (The magnified view of the device is depicted in Fig. 6b). Real-time analysis is then wirelessly transmitted to a mobile phone and viewed in a custom-developed cellphone application. The on-body assessment of sweat pH was conducted with a stationary bike for ~50 min.

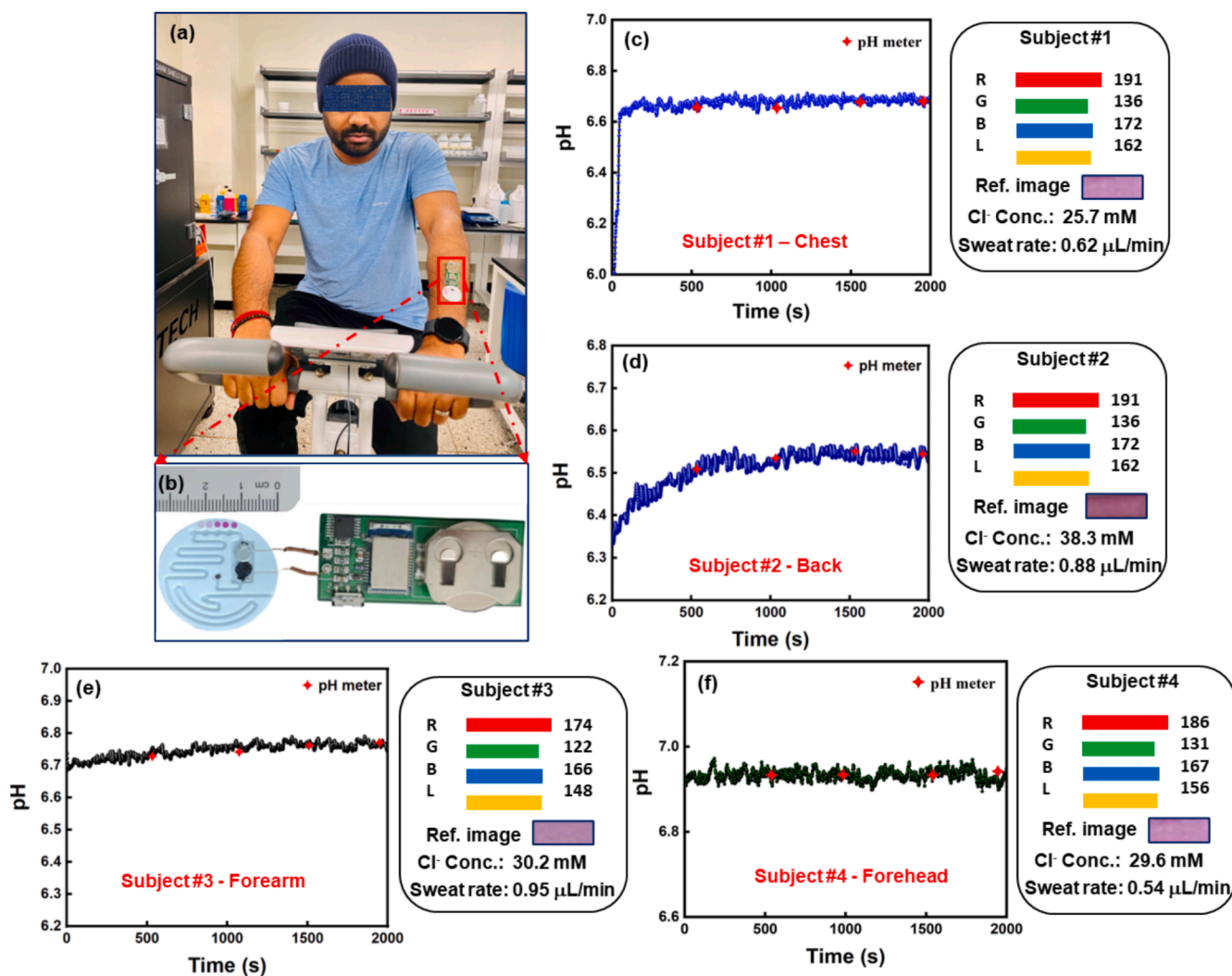


Fig. 6. Real-time and on-body analysis of human sweat. (a) displays a photographic image of a subject wearing a microfluidic wearable sensor device, accompanied by a PCB communicating with a personal mobile application, (b) an image of the complete system captured after a bout of cycling by the subject, (c-f) Real-time wirelessly acquired sweat pH value for subject #1 (Chest), subject #2 (back), subject #3 (Forearm) and subject #4 (Forehead) during a cycling exercise along with LAB color value for colorimetric measurement of chloride concentration and sweat rate.

Fig. 6(c–f) illustrate a real-time sweat pH profile relative to exercise duration, demonstrating the expected small increase in pH levels corresponding to exercise activity for subjects (#1 to #4) respectively. The increase in pH during exercise corresponds with the results of previous studies and can be attributed to the anatomy and functioning of sweat glands, as well as the presence of metabolic alkaloids [51]. Initially, the sensors exhibited no response for the first 15 min, likely due to insufficient sweat generation or incomplete filling of the electrochemical measurement chamber. After 15 min of cycling, the system started to output signals. The measured pH values were 6.6 ± 0.04 (subject #1), 6.5 ± 0.1 (subject #2), 6.7 ± 0.08 (subject #3), and 6.9 ± 0.06 (subject #4) respectively. Sweat was simultaneously collected every 500 s during cycling to compare on-body data with a commercial microelectrode pH meter, confirming the accuracy of the wearable system as shown in Fig. 6(c–f).

Further, two volunteers were given 350 mL of a soda drink with a pH of 7.8 ± 0.4 after 30 min of cycling (Fig. S20), and the sweat pH was measured both before and after consumption. The microfluidic sweat sensor was attached to the subjects' foreheads, and sweat pH was continuously monitored during the cycling activity. It was observed that the pH value of two individuals after consuming the drink was higher than before (Fig. S20). The increase in sweat pH during exercise may have been due to prolonged physical activity, which caused a significant accumulation of HCO_3^- on the skin's surface, slightly raising the sweat pH.

Further, the average chloride concentration of the sweat samples from volunteers was measured after the color development of the colorimetric assay from the device microreservoirs. Image analysis (Fig. 6) reveals that the concentration of chloride was calculated as 25.7 ± 4 mM (subject #1; chamber #1), 38.3 ± 5 mM (subject #2; chamber #2), 30.2 ± 5 mM (subject #3; chamber #1), and 29.6 ± 4 mM (subject #4; chamber #1) respectively. Further, the sweat rate was calculated as ~ 0.62 $\mu\text{L}/\text{min}$ (subject #1), ~ 0.88 $\mu\text{L}/\text{min}$ (subject #2), 0.95 $\mu\text{L}/\text{min}$ (subject #3), and 0.54 $\mu\text{L}/\text{min}$ (subject #4). These estimated chloride concentrations (Fig. 6c–f) are consistent with those obtained from a colorimetric assay conducted on sweat collected from the PDMS microfluidic device

Additionally, we calculated the local sweat loss of the volunteer's using images of microfluidic channels. The total volume of the filled microfluidic channel was determined to be 158 μL using AutoCAD 2024 software. In real-time, volunteers cycled until one or more microfluidic channels were filled with sweat. We then captured images of the filled channels, and the local sweat loss from the region was assessed across different subjects, resulting in measurements of 69.3 μL , 45.5 μL , and 87.3 μL , as shown in Fig. S21. The proposed wearable fabric-based microfluidic sensors offer numerous benefits for real-time monitoring, such as high sensitivity, portability, low cost, flexibility, and non-invasive, on-body testing. Despite these advantages, improvements are needed to make the device smaller, more affordable, reliable, durable, and capable of detecting multiple analytes in a single sweat sample.

4. Conclusion

In summary, we have devised a fabric-based microfluidic wearable sensing system that is integrated with electrochemical and colorimetric sensors, allowing for continuous real-time monitoring of sweat pH, loss, and chloride concentrations. The system comprises a disposable microfluidic device alongside reusable electrochemical sensors and an integrated wireless transceiver. In this study, the PANI electrodeposited on FCC served as the WE for pH sensing, while the Ag/AgCl@CC acted as the RE. Under optimal conditions, the portable fabric-based microfluidic pH sensor demonstrated a high sensitivity of 75.15 mV/pH along with exceptional selectivity, repeatability, and long-term stability within the sweat pH range of 2–9. As a wearable microfluidic device, the electrochemical sensing electrodes were integrated into a PCB and wirelessly connected to a smartphone to continuously measure the pH levels of

human sweat in real-time. Additionally, effective tracking of sweat loss and colorimetric readout of chloride concentration from the human subject trials during exercises was demonstrated. Consequently, the reliable and reusable proposed skin-conforming microfluidic wearable sensing systems can be readily expanded to the real-time non-invasive monitoring of sweat metabolites, paving the way for a new generation of soft electrochemical textile-based wearable microfluidic sensor systems.

CRediT authorship contribution statement

Sekar Madhu: Writing – review & editing, Writing – original draft, Validation, Methodology, Investigation, Data curation, Conceptualization. **Md.Sajjad Alam:** Validation, Software, Formal analysis. **Sriramprabha Ramasamy:** Validation, Methodology, Formal analysis. **Jungil Choi:** Writing – review & editing, Validation, Supervision, Project administration, Funding acquisition, Formal analysis, Conceptualization.

Declaration of competing interest

The authors declare that they have no known competing financial interests or personal relationships that could have appeared to influence the work reported in this paper.

Acknowledgments

The authors gratefully acknowledge the support of the National Research Foundation of Korea (NRF) grant funded by the Korean Government (Grant No. 2022R1C1C1010059), Support from the new faculty research fund of Ajou University and the Brain Pool program funded by the Ministry of Science and ICT through the NRF (NRF-2020H1D3A1A04077592).

Appendix A. Supplementary data

Supplementary data to this article can be found online at <https://doi.org/10.1016/j.cej.2024.158979>.

Data availability

Data will be made available on request.

References

- [1] M.A. Zahed, D.K. Kim, S.H. Jeong, M. Selim Reza, M. Sharifuzzaman, G.B. Pradhan, H. Song, M. Asaduzzaman, J.Y. Park, Microfluidic-integrated multimodal wearable hybrid patch for wireless and continuous physiological monitoring, *ACS Sens.* 8 (2023) 2960–2974, <https://doi.org/10.1021/acssensors.3c00148>.
- [2] G. Liu, Z. Lv, S. Batool, M.Z. Li, P. Zhao, L. Guo, Y. Wang, Y. Zhou, S.T. Han, Biocompatible material-based flexible biosensors: from materials design to wearable/implantable devices and integrated sensing systems, *Small* 19 (2023) 2207879, <https://doi.org/10.1002/sml.202207879>.
- [3] B. Ramachandran, Y.C. Liao, Microfluidic wearable electrochemical sweat sensors for health monitoring, *Biomicrofluidics* 16 (2022) 051501, <https://doi.org/10.1063/5.0116648>.
- [4] S. Madhu, A.J. Anthuuvan, S. Ramasamy, P. Manickam, S. Bhansali, P. Nagamony, V. Chinnuswamy, ZnO nanorod integrated flexible carbon fibers for sweat cortisol detection, *ACS Appl. Electron. Mater.* 2 (2020) 499–509, <https://doi.org/10.1021/acsaem.9b00730>.
- [5] R. Ghaffari, J. Choi, M.S. Raj, S. Chen, S.P. Lee, J.T. Reeder, A.J. Aranyosi, A. Leech, W. Li, S. Schon, J.B. Model, J.A. Rogers, Soft wearable systems for colorimetric and electrochemical analysis of biofluids, *Adv. Funct. Mater.* 30 (2020) 1907269, <https://doi.org/10.1002/adfm.201907269>.
- [6] H. Cao, R. Lin, Z. Long, L. Xing, X. Xue, A self-powered wireless sweat-analysis patch for real-time monitoring physiological status, *Nano Energy* 123 (2024) 109411, <https://doi.org/10.1016/j.nanoen.2024.109411>.
- [7] M. Sharifuzzaman, A. Chhetry, M.A. Zahed, S.H. Yoon, C.I. Park, S. Zhang, S. Chandra Barman, S. Sharma, H. Yoon, J.Y. Park, Smart bandage with integrated multifunctional sensors based on MXene-functionalized porous graphene scaffold for chronic wound care management, *Biosens. Bioelectron.* 169 (2020) 112637, <https://doi.org/10.1016/j.bios.2020.112637>.

- [8] T. Saha, R. Del Caño, E. De la Paz, S.S. Sandhu, J. Wang, Access and management of sweat for non-invasive biomarker monitoring: a comprehensive review, *Small* 19 (2023) 2206064, <https://doi.org/10.1002/smll.202206064>.
- [9] A.J. Bandodkar, V.W.S. Hung, W. Jia, G. Valdés-Ramírez, J.R. Windmiller, A. G. Martínez, J. Ramírez, G. Chan, K. Kerman, J. Wang, Tattoo-based potentiometric ion-selective sensors for epidermal pH monitoring, *Analyst* 138 (2013) 123–128, <https://doi.org/10.1039/c2an36422k>.
- [10] Q. Tao, S. Liu, J. Zhang, J. Jiang, Z. Jin, Y. Huang, X. Liu, S. Lin, X. Zeng, X. Li, G. Tao, H. Chen, Clinical applications of smart wearable sensors, *iScience* 26 (2023) 107485, <https://doi.org/10.1016/j.isci>.
- [11] J. Gonzalo-Ruiz, R. Mas, C. de Haro, E. Cabruja, R. Camero, M.A. Alonso-Lomillo, F.J. Muñoz, Early determination of cystic fibrosis by electrochemical chloride quantification in sweat, *Biosens. Bioelectron.* 24 (2009) 1788–1791, <https://doi.org/10.1016/j.bios.2008.07.051>.
- [12] J. Kim, S. Oh, D.S. Yang, L. Rugg, R. Mathur, S.S. Kwak, S. Yoo, S. Li, E. Kanatzidis, G. Lee, H.J. Yoon, Y. Huang, R. Ghaffari, S.A. McColley, J.A. Rogers, A skin-interfaced, miniaturized platform for triggered induction, capture and colorimetric multicomponent analysis of microliter volumes of sweat, *Biosens. Bioelectron.* 253 (2024) 116166, <https://doi.org/10.1016/j.bios.2024.116166>.
- [13] J. Kim, S. Lee, S. Kim, M. Jung, H. Lee, M.S. Han, Development of a fluorescent chemosensor for chloride ion detection in sweat using Ag⁺-benzimidazole complexes, *Dyes Pigm.* 177 (2020) 108291, <https://doi.org/10.1016/j.dyepig.2020.108291>.
- [14] W. Nikolajek, H. Emrich, *Klinische Wochenschrift* pH of sweat of patients with cystic fibrosis, *Klin Wschr.* 54 (1976) 287–288, <https://doi.org/10.1007/BF01468925>.
- [15] L. Wei, Z. Lv, Y. He, L. Cheng, Y. Qiu, X. Huang, C. Ding, H. Wu, A. Liu, In-situ admittance sensing of sweat rate and chloride level in sweat using wearable skin-interfaced microfluidic patch, *Sens. Actuators B Chem.* 379 (2023) 133213, <https://doi.org/10.1016/j.snb.2022.133213>.
- [16] R.P. Nuccio, K.A. Barnes, J.M. Carter, L.B. Baker, Fluid balance in team sport athletes and the effect of hypohydration on cognitive, technical, and physical performance, *Sports Med.* 47 (2017) 1951–1982, <https://doi.org/10.1007/s40279-017-0738-7>.
- [17] A.M.V. Mohan, V. Rajendran, R.K. Mishra, M. Jayaraman, Recent advances and perspectives in sweat based wearable electrochemical sensors, *TRAC – Trends Anal. Chem.* 131 (2020) 116024, <https://doi.org/10.1016/j.trac.2020.116024>.
- [18] S. Madhu, S. Ramasamy, P. Manickam, P. Nagamony, V. Chinnuswamy, TiO₂ anchored carbon fibers as non-invasive electrochemical sensor platform for the cortisol detection, *Mater. Lett.* 308 (2022) 131238, <https://doi.org/10.1016/j.matlet.2021.131238>.
- [19] C.W. Bae, P.T. Toi, B.Y. Kim, W. Il Lee, H.B. Lee, A. Hanif, E.H. Lee, N.E. Lee, Fully stretchable capillary microfluidics-integrated nanoporous gold electrochemical sensor for wearable continuous glucose monitoring, *ACS Appl. Mater. Interfaces* 11 (2019) 14567–14575, <https://doi.org/10.1021/acami.9b00848>.
- [20] S. Madhu, S. Ramasamy, V. Magudeeswaran, P. Manickam, P. Nagamony, V. Chinnuswamy, SnO₂ nanoflakes deposited carbon yarn-based electrochemical immunosensor towards cortisol measurement, *J. Nanostruct. Chem.* 13 (2023) 115–127, <https://doi.org/10.1007/s40097-022-00486-1>.
- [21] S. Madhu, J.H. Han, C.W. Jeong, J. Choi, Sensitive electrochemical sensing platform based on Au nanoflower-integrated carbon fiber for detecting interleukin-6 in human serum, *Anal. Chim. Acta* 1238 (2023), <https://doi.org/10.1016/j.aca.2022.340644>.
- [22] R. Vinoth, T. Nakagawa, J. Mathiyarasu, A.M.V. Mohan, Fully Printed wearable microfluidic devices for high-throughput sweat sampling and multiplexed electrochemical analysis, *ACS Sens.* 6 (2021) 1174–1186, <https://doi.org/10.1021/acssensors.0c02446>.
- [23] S. Zhang, M.A. Zahed, M. Sharifuzzaman, S. Yoon, X. Hui, S. Chandra Barman, S. Sharma, H.S. Yoon, C. Park, J.Y. Park, A wearable battery-free wireless and skin-interfaced microfluidics integrated electrochemical sensing patch for on-site biomarkers monitoring in human perspiration, *Biosens. Bioelectron.* 175 (2021) 112844, <https://doi.org/10.1016/j.bios.2020.112844>.
- [24] G. de Marzo, V.M. Mastroradi, M.T. Todaro, L. Blasi, V. Antonaci, L. Algeri, M. Scaraggi, M. De Vittorio, Sustainable electronic biomaterials for body-compliant devices: challenges and perspectives for wearable bio-mechanical sensors and body energy harvesters, *Nano Energy* 123 (2024), <https://doi.org/10.1016/j.nanoen.2024.109336>.
- [25] D. Li, Y. Feng, F. Li, J. Tang, T. Hua, Carbon fibers for bioelectrochemical precursors, bioelectrochemical system, and biosensors, *Adv. Fiber Mater.* 5 (2023) 699–730, <https://doi.org/10.1007/s42765-023-00256-w>.
- [26] M. Sekar, M. Pandiaraj, S. Bhansali, N. Ponpandian, C. Viswanathan, Carbon fiber based electrochemical sensor for sweat cortisol measurement, *Sci. Rep.* 9 (2019) 403, <https://doi.org/10.1038/s41598-018-37243-w>.
- [27] P. Manickam, S. Madhu, R.E. Fernandez, C. Viswanathan, S. Bhansali, Fabric based wearable biosensor for continuous monitoring of steroids, *ECS Trans.* 77 (2017) 1841–1846, <https://doi.org/10.1149/07711.1841ecst>.
- [28] J. Kim, A.S. Campbell, B.E.F. de Ávila, J. Wang, Wearable biosensors for healthcare monitoring, *Nat. Biotechnol.* 37 (2019) 389–406, <https://doi.org/10.1038/s41587-019-0045-y>.
- [29] M. Sekar, R. Sriramprabha, P.K. Sekhar, S. Bhansali, N. Ponpandian, M. Pandiaraj, C. Viswanathan, Review—towards wearable sensor platforms for the electrochemical detection of cortisol, *J. Electrochem. Soc.* 167 (2020) 067508, <https://doi.org/10.1149/1945-7111/ab7e24>.
- [30] Z. Zhao, Q. Li, L. Chen, Y. Zhao, J. Gong, Z. Li, J. Zhang, A thread/fabric-based band as a flexible and wearable microfluidic device for sweat sensing and monitoring, *Lab. Chip* 21 (2021) 916–932, <https://doi.org/10.1039/d0lc01075h>.
- [31] H.Y.Y. Nyein, L.C. Tai, Q.P. Ngo, M. Chao, G.B. Zhang, W. Gao, M. Bariya, J. Bullock, H. Kim, H.M. Fahad, A. Javey, A wearable microfluidic sensing patch for dynamic sweat secretion analysis, *ACS Sens.* 3 (2018) 944–952, <https://doi.org/10.1021/acssensors.7b00961>.
- [32] Y. Zhang, H. Guo, S.B. Kim, Y. Wu, D. Ostojich, S.H. Park, X. Wang, Z. Weng, R. Li, A.J. Bandodkar, Y. Sekine, J. Choi, S. Xu, S. Quaggin, R. Ghaffari, J.A. Rogers, Passive sweat collection and colorimetric analysis of biomarkers relevant to kidney disorders using a soft microfluidic system, *Lab. Chip* 19 (2019) 1545–1555, <https://doi.org/10.1039/c9lc00103d>.
- [33] J.R. Sempionatto, I. Jeerapan, S. Krishnan, J. Wang, Wearable chemical sensors: emerging systems for on-body analytical chemistry, *Anal. Chem.* 92 (2019) 378–396, <https://doi.org/10.1021/acs.analchem.9b04668>.
- [34] A.J. Bandodkar, P. Gutruf, J. Choi, K. Lee, Y. Sekine, J.T. Reeder, W.J. Jeang, A. J. Aranyosi, S.P. Lee, J.B. Model, R. Ghaffari, C.-J. Su, J.P. Leshock, T. Ray, A. Verrillo, K. Thomas, V. Krishnamurthi, S. Han, J. Kim, S. Krishnan, T. Hang, J. A. Rogers, Battery-free, skin-interfaced microfluidic/electronic systems for simultaneous electrochemical, colorimetric, and volumetric analysis of sweat, *Sci. Adv.* 5 (2019) 3294, <https://www.science.org>.
- [35] M.S. Hossain, N. Padmanathan, M.M.R. Badal, K.M. Razeeb, M. Jamal, Highly sensitive potentiometric pH sensor based on polyaniline modified carbon fiber cloth for food and pharmaceutical applications, *ACS Omega* 9 (2024) 40122, <https://doi.org/10.1021/acsomega.4c06090>.
- [36] T. Guinovart, G.A. Crespo, F.X. Rius, F.J. Andrade, A reference electrode based on polyvinyl butyral (PVB) polymer for decentralized chemical measurements, *Anal. Chim. Acta* 821 (2014) 72–80, <https://doi.org/10.1016/j.aca.2014.02.028>.
- [37] A.M. Zamarayeva, N.A.D. Yamamoto, A. Toor, M.E. Payne, C. Woods, V.I. Pister, Y. Khan, J.W. Evans, A.C. Arias, Optimization of printed sensors to monitor sodium, ammonium, and lactate in sweat, *APL Mater.* 8 (2020) 100905, <https://doi.org/10.1063/5.0014836>.
- [38] J. Choi, A.J. Bandodkar, J.T. Reeder, T.R. Ray, A. Turnquist, S.B. Kim, N. Nyberg, A. Hourlier-Fargette, J.B. Model, A.J. Aranyosi, S. Xu, R. Ghaffari, J.A. Rogers, Soft, skin-integrated multifunctional microfluidic systems for accurate colorimetric analysis of sweat biomarkers and temperature, *ACS Sens.* 4 (2019) 379–388, <https://doi.org/10.1021/acssensors.8b01218>.
- [39] M.S. Alam, J.K. Kim, J. Choi, Multifunctional wearable system for mapping body temperature and analyzing sweat, *ACS Sens.* 8 (2023) 1980–1988, <https://doi.org/10.1021/acssensors.3c00098>.
- [40] D. Liu, Z. Liu, S. Feng, Z. Gao, R. Chen, G. Cai, S. Bian, Wearable microfluidic sweat chip for detection of sweat glucose and pH in long-distance running exercise, *Biosensors (Basel)* 13 (2023) 157, <https://doi.org/10.3390/bios13020157>.
- [41] S. Madhu, P. Manickam, M. Pierre, S. Bhansali, P. Nagamony, V. Chinnuswamy, Nanostructured SnO₂ integrated conductive fabrics as binder-free electrode for neurotransmitter detection, *Sens. Actuators A Phys* 269 (2018) 401–411, <https://doi.org/10.1016/j.sna.2017.11.046>.
- [42] J. Li, L. Zhao, P. Liu, One-step electrodeposition of polyaniline nanorods on carbon cloth for high-performance flexible supercapacitors, *Langmuir* 39 (2023) 14297–14307, <https://doi.org/10.1021/acs.langmuir.3c01594>.
- [43] W. Kong, S. Yi, W. Sun, L. Xu, L. Jia, D. Yan, Z. Li, Poly(aniline)-decorated carbon fibers for enhanced mechanical and electromagnetic interference shielding performances of epoxy composites, *Mater. Des.* 217 (2022) 110658, <https://doi.org/10.1016/j.matdes.2022.110658>.
- [44] H. Peng, G. Ma, K. Sun, J. Mu, X. Zhou, Z. Lei, A novel fabrication of nitrogen-containing carbon nanospheres with high rate capability as electrode materials for supercapacitors, *RSC Adv.* 5 (2015) 12034–12042, <https://doi.org/10.1039/c4ra11889h>.
- [45] M. Pierre, S. RoyChoudhury, Y. Umasankar, P. Manickam, R.E. Fernandez, N. Munroe, S. Bhansali, Textile fiber electrode to monitor uric acid and for assessing wound chronicity, *ECS Trans.* 80 (2017) 1277–1286, <https://doi.org/10.1149/08010.1277ecst/meta>.
- [46] H.J. Park, J.H. Yoon, K.G. Lee, B.G. Choi, Potentiometric performance of flexible pH sensor based on polyaniline nanofiber arrays, *Nano Converg.* 6 (2019) 9, <https://doi.org/10.1186/s40580-019-0179-0>.
- [47] R. Rahimi, M. Ochoa, T. Parupudi, X. Zhao, I.K. Yazdi, M.R. Dokmeci, A. Tamayol, A. Khademhosseini, B. Ziaie, A low-cost flexible pH sensor array for wound assessment, *Sens. Actuators B Chem.* 229 (2016) 609–617, <https://doi.org/10.1016/j.snb.2015.12.082>.
- [48] J. Zhou, B. Jiang, C. Gao, K. Zhu, W. Xu, D. Song, Stable, reusable, and rapid response smart pH-responsive cotton fabric based on covalently immobilized with naphthalimide-rhodamine probe, *Sens. Actuators B Chem.* 355 (2022) 131310, <https://doi.org/10.1016/j.snb.2021.131310>.
- [49] G. Bolat, E. De la Paz, N.F. Azeredo, M. Kartolo, J. Kim, A.N. de Loyola e Silva, R. Rueda, C. Brown, L. Angnes, J. Wang, J.R. Sempionatto, Wearable soft electrochemical microfluidic device integrated with iontophoresis for sweat biosensing, *Anal. Bioanal. Chem.* 414 (2022) 5411–5421, <https://doi.org/10.1007/s00216-021-03865-9>.
- [50] K. Krorakai, S. Klangphukhiew, S. Kulchat, R. Patramanon, Smartphone-based NFC potentiostat for wireless electrochemical sensing, *Appl. Sci.* (2021) 1–13, <https://doi.org/10.3390/app11010392>.
- [51] K. Kwon, J.U. Kim, Y. Deng, S.R. Krishnan, J. Choi, H. Jang, K.H. Lee, C.J. Su, I. Yoo, Y. Wu, L. Lipschultz, J.H. Kim, T.S. Chung, D. Wu, Y. Park, T. Il Kim, R. Ghaffari, S. Lee, Y. Huang, J.A. Rogers, An on-skin platform for wireless monitoring of flow rate, cumulative loss and temperature of sweat in real time, *Nat. Electron.* 4 (2021) 302–312, <https://doi.org/10.1038/s41928-021-00556-2>.
- [52] M.L. Zamora, J.M. Dominguez, R.M. Trujillo, C.B. Goy, M.A. Sánchez, R.E. Madrid, Potentiometric textile-based pH sensor, *Sens. Actuators B Chem.* 260 (2018) 601–608, <https://doi.org/10.1016/j.snb.2018.01.002>.

- [53] L. Manjakkal, W. Dang, N. Yogeswaran, R. Dahiya, Textile-based potentiometric electrochemical PH sensor for wearable applications, *Biosensors* 9 (2019) 14, <https://doi.org/10.3390/bios9010014>.
- [54] R. Wang, Q. Zhai, Y. Zhao, T. An, S. Gong, Z. Guo, Q.Q. Shi, Z. Yong, W. Cheng, Stretchable gold fiber-based wearable electrochemical sensor toward pH monitoring, *J. Mater. Chem. B* 8 (2020) 3655–3660, <https://doi.org/10.1039/c9tb02477h>.
- [55] L. Possanzini, F. Decataldo, F. Mariani, I. Gualandi, M. Tessarolo, E. Scavetta, B. Fraboni, Textile sensors platform for the selective and simultaneous detection of chloride ion and pH in sweat, *Sci. Rep.* 10 (2020) 17180, <https://doi.org/10.1038/s41598-020-74337-w>.
- [56] Y. Wang, H. Guo, M. Yuan, J. Yu, Z. Wang, X. Chen, One-step laser synthesis platinum nanostructured 3D porous graphene: a flexible dual-functional electrochemical biosensor for glucose and pH detection in human perspiration, *Talanta* 257 (2023) 124362, <https://doi.org/10.1016/j.talanta.2023.124362>.
- [57] M. Hu, Z. Wang, L. Zhang, S. Lin, J. Liao, A microfluidic patch for wireless wearable electrochemical detection of sweat metabolites, *Sens. Actuators B Chem.* 422 (2025) 136604, <https://doi.org/10.1016/j.snb.2024.136604>.
- [58] L. Chen, F. Chen, G. Liu, H. Lin, Y. Bao, D. Han, W. Wang, Y. Ma, B. Zhang, L. Niu, Superhydrophobic functionalized Ti3C2Tx MXene-based skin-attachable and wearable electrochemical pH sensor for real-time sweat detection, *Anal. Chem.* 94 (2022) 7319–7328, <https://doi.org/10.1021/acs.analchem.2c00684>.
- [59] H.Y.Y. Nyein, W. Gao, Z. Shahpar, S. Emaminejad, S. Challa, K. Chen, H.M. Fahad, L.C. Tai, H. Ota, R.W. Davis, A. Javey, A wearable electrochemical platform for noninvasive simultaneous monitoring of Ca²⁺ and pH, *ACS Nano* 10 (2016) 7216–7224, <https://doi.org/10.1021/acsnano.6b04005>.
- [60] L. Fiore, V. Mazzaracchio, A. Antinucci, R. Ferrara, T. Sciarra, F. Lista, A.Q. Shen, F. Arduini, Wearable electrochemical device based on butterfly-like paper-based microfluidics for pH and Na⁺ monitoring in sweat, *Microchim. Acta* 191 (2024) 580, <https://doi.org/10.1007/s00604-024-06564-1>.
- [61] H. Zhao, X. Zhang, Y. Qin, Y. Xia, X. Xu, X. Sun, D. Yu, S.M. Mugo, D. Wang, Q. Zhang, An integrated wearable sweat sensing patch for passive continuous analysis of stress biomarkers at rest, *Adv. Funct. Mater.* 33 (2023) 2212083, <https://doi.org/10.1002/adfm.202212083>.
- [62] S.Y. Oh, S.Y. Hong, Y.R. Jeong, J. Yun, H. Park, S.W. Jin, G. Lee, J.H. Oh, H. Lee, S. S. Lee, J.S. Ha, Skin-attachable, stretchable electrochemical sweat sensor for glucose and pH detection, *ACS Appl. Mater. Interfaces* 10 (2018) 13729–13740, <https://doi.org/10.1021/acsami.8b03342>.
- [63] Y. Zhao, Y. Yu, S. Zhao, R. Zhu, J. Zhao, G. Cui, Highly sensitive pH sensor based on flexible polyaniline matrix for synchronal sweat monitoring, *Microchem. J.* 185 (2023) 108092, <https://doi.org/10.1016/j.microc.2022.108092>.